Preprint of accepted manuscript: Chafer, C., Santin, C. & Doerr, S.H. (2016) Modelling and quantifying the spatial distribution of post-wildfire ash loads. *International Journal of Wildland Fire* 25, 249-255. (*doi:10.1071/WF15074*).

Modelling and quantifying the spatial distribution of post-wildfire ash loads

Chris J. Chafer [a*], Cristina Santín [b], Stefan H. Doerr [b]

[a] WaterNSW, Penrith, Australia

[b] Geography Department, Swansea University, Swansea, United Kingdom

(* corresponding author chris.chafer@waternsw.com.au)

Abstract

Ash is generated in every wildfire, but its eco-hydro-geomorphic effects remain poorly understood and quantified, especially at large spatial scales. Here we present a new method that allows modelling the spatial distribution of ash loads in the post-fire landscape. Based on a severe wildfire that burnt ~13,600 ha of a forested water supply catchment in October 2013 (2013 Hall Road Fire, 100km south west of Sydney, Australia), Based on an existing spectral ratio-based index, we developed a new spectral index using Landsat 8 satellite imagery: the normalized wildfire ash index (NWAI). Before- and after-fire images were normalised and a differenced wildfire ash image (dNWAI) computed. The relationship between dNWAI and ash loads (t ha^{-1}) quantified *in situ* at nine sampling locations burnt under a range of fire severities was determined using a polynomial regression (R^2=0.98). A spatially applied model was computed within a Geographic Information System (GIS) to illustrate the spatial distribution of ash across the area burnt and to estimate ash loads in the five subcatchments affected by the wildfire. Approximately 181,000 tons of ash was produced by the wildfire with specific loads increasing with fire severity. This new tool to model wildfire ash distribution can inform decisions about post-fire land management in future wildfires in the region. It can also be adapted for its application in other fire-prone environments.

Short summary

We present a new methodology that allowed modelling the amount and spatial distribution of wildfire ash (t ha^{-1}) in a burnt SE-Australian eucalypt forest. This tool can be applied in the region, and, if adapted, elsewhere, to inform post-fire land management for mitigating impacts from ash, such as debris flows or water contamination.

Additional keywords: fire severity, post-fire erosion, water contamination, eucalypt forest, wildfire.

Introduction

Wildfires can produce post-fire conditions that can result in serious risk to drinking water supply (Smith *et al.* 2011). The main water contamination risk derived from fire is the enhancement of water erosion leading to sediment transfer to drainage lines and water storage reservoirs (Shakesby and Doerr 2006; Malvar *et al.* 2011). Beside eroded soil, wildfire ash is one of the main components of the post-fire sediment (Smith *et al.* 2011). Ash can be defined as the particulate residue remaining, or deposited on the ground, from the burning of wildland fuels and consisting of mineral materials and charred organic components (Bodí *et al*. 2014). Ash can have high concentrations of potential water pollutants such as nutrients or carcinogenic organic compounds (Goforth *et al.* 2005; Santín *et al.* 2012).

The intrinsic properties of ash have been examined for a range of fire types and ecosystems (e.g. Liodakis *et al.* 2005; Bodí *et al.* 2011; Balfour *et al.* 2014; Pereira *et al.* 2014); however its eco-hydro-geomorphic effects remain poorly quantified (Bodí *et al.* 2014). A fundamental step in that direction is to understand ash production and distribution at the landscape-scale. Knowledge of ash quantity, type and characteristics at large scales (e.g. fire-affected catchments or entire areas burnt) would not only allow better evaluation of overall wildfire impacts but also incorporation of ash as a new parameter into post-fire risk models (Moody *et al.* 2014). Several studies have examined the spectral properties of wildfire ash using satellite imagery or aerial and hand-held multispectral and hyperspectral sensors (Landmann 2003; Kokaly *et al*. 2007; Lewis *et al*. 2007; Lugassi *et al.* 2009; Smith *et al.* 2010; Lewis *et al.* 2011; Vincentie 2012). Results from those studies (both field and laboratory-based) indicate that significant spectral differences occur between the near infra-red (NIR) and short-wave infra-red (SWIR) parts of the spectrum as ash load increases. Additionally, it has been shown that the standard fire severity indexes (NBR and dNBR) are ineffective in evaluating ash load (Smith *et al.* 2010). Although remote sensing provides a potential to monitor and analyse the spatial and temporal properties of wildfire ash, few studies have addressed this subject (Smith and Hudak 2005; Kokaly *et al*. 2007), and none appear to have investigated the spatial distribution of post-fire wildfire ash loads (Bodí *et al.* 2014). Here we propose a method to

60 quantify and illustrate the spatial distribution of wildfire ash loads using satellite imagery,
61 applied to a eucalypt forest fire in SE Australia.

62

Methods

Study area and site selection

This study focuses on the area affected by the Hall Road wildfire, Balmoral (17 October 2013, SW of Sydney, Australia; Fig. 1). It burnt nearly 16,000 ha including 13,588 ha of forested drinking water supply catchment managed by Water NSW (Murphy 2014). The study area had not burnt since a controlled fuel reduction burn in October 1996. The climate here is humid temperate, with annual rainfall of 900-1000 mm. Soils are sandy to sandy clay loam-textured Cambisols, developed over quartzitic Hawkesbury Sandstone with shale outcrops (Doerr *et al.* 2006; FAO 2014). Deep canyons and gorges with intervening ridges and gently-sloping plateaus characterise the landscape, with the dominant vegetation being dry eucalypt forest with a dense shrubby understorey (Keith 2006).

Sampling sites were selected along seven kilometres of a ridge typical of the region (Fig. 1) with a relatively homogeneous fuel load of 25-30 t ha^{-1}, estimated as per Chafer *et al.* (2004), and comprising ground, shrub, bark and canopy fuels <1 cm diameter. Dominant canopy vegetation comprised of eucalypts (*Eucalyptus* sp) with a shrub layer up to 4 m high dominated by *Banksia* sp, *Leptospernum* sp, *Acacia* sp and *Petrophile* sp. Despite the terrain homogeneity, wind-driven differences in fire behaviour (winds greater than 45 km h^{-1} and blowing perpendicular to the orientation of the ridge, i.e., westerly winds; Murphy 2014) resulted in a range of fire severities along the length of the ridge (Fig. 1). This provided an ideal context to examine ash production in relatively homogenous areas impacted by different fire severities. Fire severity was determined based on the degree of consumption of vegetation and ground fuels (see *Fire severity* subsection).

Ash was sampled at sites affected by low, high and extreme fire severities, which covered the whole range of fire severity classes identified in the burnt area (see *Fire severity* subsection*)*. All sites were selected in flat areas (slope angles 0-2.5º) to minimise any risk of redistribution of the ash by water erosion between the fire and sampling (85 days after the fire). Total rainfall between the wildfire and sampling was 148 mm, with a maximum daily precipitation of 31 mm (data from the nearby Buxton Station N.068166). No signs of post-fire

redistribution of ash by water erosion were evident at the study sites. However, some redistribution of ash via wind and leaching is likely to have occurred during and after the fire (Santín *et al*. 2015).

Field sampling procedure

For each of the three fire severity classes sampled (separated by up to two km each), three comparable sites were selected as replicates (Fig 1.). At each replicate site, three parallel transects (18 m long and 6 m apart) were laid out in the direction of the fire propagation (W-E). At each transect, 10 sampling points (every 2 m) resulting in a total of 30 sampling points per site (i.e. 90 per fire severity class). At each sampling point, the ash layer was collected with a brush from a square of 400 to 600 cm^2 (size depending on ash load). This non-cohesive material consisted of burnt residues from litter, understory and overstorey, together with burnt surface mineral soil which had lost its structure and became part of the ash itself (Santín *et al*. 2015). At the time of sampling, materials >1 cm were removed as well as unburnt matter that had fallen to the ground after the fire. The weights of air-dried samples were recorded using a two-figure balance and ash loads determined for each sampling point. Further details of field sampling procedures and of ash chemical characteristics are given in Santín *et al*. (2015).

Satellite Imagery

Landsat 8 imagery was obtained over the study area immediately before the wildfire (11 October 2013), immediately after the wildfire (05 November 2013) and at the time of field sampling (02 January 2014) from the U.S. Geological Survey archives using EarthExplorer. Imagery was radiometrically and atmospherically corrected within ERDAS Imagine image processing software (Hexagon 2015) using standard top of the atmosphere processing algorithms (USGS 2015) and a standard Lamberts conformal conic projection in Geographic Datum of Australia (GDA94) to 25 m^2 pixels (cells).

Fire severity

Wildfire severity was computed across the study area from the October and November 2013 Landsat 8 imagery using the standard differenced Normalized Burn Ratio (*dNBR*) (Key 2006) and field-based severity classes defined through the area burnt as per Chafer (2008):

126 $$dNBR = NBR_{prefire} - NBR_{postfire} \quad \textit{eq. 1.}$$

127 $$\text{where } NBR = (p0.85 - p2.21) / (p0.85 + p2.21) \quad \textit{eq. 2.}$$

128 Where *p*0.85 is the near-infrared (NIR) band 5 and *p*2.21 is the shortwave infrared (SWIR-2)
129 band 7 of the Landsat 8 satellite platform (NASA 2010).

130 The fire severity range found was divided into the following six fire severity classes using the
131 criteria of Chafer (2008), dNBR ranged from -115 to 1,126. Cut off values for each class are
132 provided:

133 *i)* *Unburnt:* area unaffected by the fire. dNBR <140
134 *ii)* *Low fire severity:* ground and understory (<0.5 m high) fuels burnt, down woody
135 debris scorched. Canopy unaffected. dNBR 140-240
136 *iii)* *Moderate fire severity:* ground and understory (<4 m high) fuels burnt, down woody
137 debris scorched. Canopy unaffected. dNBR 240-440
138 *iv)* *High fire severity*: ground, down wood and understory (<4 m high) fuels consumed.
139 Canopy scorched. dNBR 440-610
140 *v)* *Very high severity*: all available fuels consumed, including stems <0.5 cm thick.
141 dNBR 610-890
142 *vi)* *Extreme fire severity*: all available fuels consumed, including stems <1cm thick.
143 dNBR >890
144
145 The statistical validity of this classification was examined for normality and the raw dNBR
146 values tested using a one-factor ANOVA from 500 randomly generated points (Fig 3)..
147 Tukey's post-hoc pairwise comparisons were used to test differences between severity
148 classes. The level of significance used for all tests was 5% (i.e. $\alpha = 0.05$).

149 *Wildfire-derived ash index*
150 To interpret the spatial distribution of ash load, a new spectral index, the 'Normalised
151 Wildfire Ash Index' (NWAI), was developed using two spectral bands in the 0.84 to 1.66 µm
152 range. Examination of spectral signatures from the study area suggested that pre- and post-
153 fire differences in NIR and SWIR-1 (Fig. 2) might produce a useful criterion for analysing
154 the distribution of ash loads across the area burnt. Given that ash absorbs solar energy within
155 the 0.84-1.66 µm range (Fig. 2), the NWAI was designed to capitalize on spectral properties

within that wavelength range. As there may have been some ash redistributed through wind erosion and leaching between the fire and sampling time (see Santín *et al.* 2015), we used an October 2013 (pre-fire) and a January 2014 (post-fire, at time of field sampling) images to develop the proposed ash index (NWAI).

NWAI uses the Normalised Difference Infrared Index (NDII) (Hardisky *et al*. 1983; Yilmaz *et al.* 2008; Datt 2009, Wang *et al.* 2013), which is derived from Landsat 8 satellite data using:

$$NDII = (p0.85 - p1.65) / (p0.85 + p1.65) \quad \text{eq. 3.}$$

Where $p0.85$ is the near infrared (NIR) band 5 and $p1.65$ is the shortwave infrared (SWIR-1) band 6 of the Landsat 8 satellite platform (NASA 2010).

NDII fundamentally reports on a combination of vegetation stress, bare soil and moisture content (Yilmaz *et al*. 2008; Datt 2009).

NWAI is the NDII standardised to range between 0 and 1 from data only within the boundary of the area burnt:

$$NWAI = (NDII_i - NDII_{min}) / (NDII_{max} - NDII_{min}) \quad \text{eq. 4.}$$

Where $NDII_i$ is the value of each cell in the image, $NDII_{min}$ is the minimum value and $NDII_{max}$ is the maximum value within the area burnt.

The NWAI is computed only within the area burnt for two satellite images, one captured before and one after the wildfire. They are then normalised (eq. 4) and differenced:

$$dNWAI = 0.05 + ((NWAI_{prefire} - NWAI_{postfire})/(NWAI_{prefire} + NWAI_{postfire})) \quad \text{eq. 5.}$$

Ash absorbs solar energy within the 0.84–1.66 μm range. This is illustrated by the index, with higher values (i.e. approaching 1) in the areas where vegetation has been more intensely affected by the fire and more ash has been produced. Data is standardised as per eq. 4 to range between 0 and 1, where 1 approximates the highest total ash load from the area burnt and 0 is unburnt vegetation.

A paired sample *t-test* was used to test differences in NWAI from 500 randomly generated points (Fig 3) for the pre- and post-fire images in the different fire severity classes.

183

184 *Modelling ash loads*

185 To assess the spatial distribution of ash (i.e. ash loads) across the area burnt using the dNWAI
186 for each of the nine burnt sampling sites, plus two randomly-selected unburnt control sites,
187 we obtained a statistical regression relationship between the values of dNWAI and the
188 average ash loads (t ha^{-1}) measured at these sites (Fig. 3 insert). Within ArcGIS we applied
189 the subsequently derived regression equation to the dNWAI for every 25 m^2 pixel (ignoring
190 unburnt pixels which would have zero ash). In this way, ash loads were computed within the
191 GIS for all the fire severity classes in the whole area burnt and, thus, the total amount of ash
192 generated was estimated (Fig. 3). This also allowed calculating ash loads for each severity
193 class in each of the fire-affected subcatchments (see table in Fig. 3).

194

195 **Results and Discussion**

196 Using the raw dNBR from the 500 randomly generated points across the burnt area, there was
197 a significant difference between the six fire severity class means (Fig 1) (ANOVA F=933.7,
198 P<0.001) and a Tukey's post-hoc pairwise comparisons demonstrated all classes had
199 significantly different means. These class differences demonstrate the usefulness of the
200 severity classification methodology in south-eastern Australian environments for quantifying
201 the degree of vegetation destruction (for rationale and validation see Chafer *et al.* 2004 and
202 Chafer 2008). From the dNBR image we choose field locations to collect the ash samples.

203 The total ash loads quantified in the field sampling sites ranged from 6 ±0.7 t ha^{-1} for low
204 severity, 15.9 ±0.9 t ha^{-1} for high severity and 34.2 ±2.1 t ha^{-1} for extreme severity (arithmetic
205 mean ±standard error of mean; n = 90). The spectral properties from the sampling sites and
206 90 random points from unburnt and extreme severity (Fig. 2) suggested that using Landsat 8
207 NIR and SWIR-1 data might provide useful results for examining ash load. SWIR-1 showed
208 only minimal change through time in burnt pixels, regardless of severity (Fig. 2c), whereas
209 SWIR-2 changed significantly after being burnt (Fig. 2d). Thus SWIR-1was used to
210 normalize against NIR to create dNWAI (using eq. 3,4,5) (see also Smith *et al.* 2010). The
211 subsequent analysis of 500 random points distributed throughout the burnt area showed that
212 NWAI values were not significantly different pre- and post-fire for unburnt areas (n=38,
213 t=0.894, P=0.377). However, for the areas burnt under the remaining range of fire severities,

all showed significant differences in the NWAI pre- and post-fire (low severity: n=92, t=10.5, P=0.001, mod. severity n=147, t=27.9, P<0.001, high severity n=134, t=55.8, P<0.001, very high severity n=62, t=53.5, P<0.001, extreme severity n=28, t=64.4, P<0.001). This indicates that using NIR and SWIR-1 and then standardising NWAI values to range between 0 and 1, is a potentially useful method of comparing ash data from the two dates.

A significant positive relationship was found between the dNWAI values and the average ash loads measured at the sampling sites (R^2=0.988; Fig. 3 insert). The highest values of dNWAI (i.e. approaching 0.6), and the highest ash loads, were obtained in the areas where vegetation had been most severely burnt (i.e. extreme fire severity), whereas the control unburnt sites showed values very close to zero (Fig. 3 insert).

The spatial distribution of the ash loads is shown in Fig. 3. The results infer that the Hall Road wildfire led to the deposition of ash in the order of 181,000 tons (table insert in Fig 3), with ash loads increasing with increased fire severity (Fig. 3). In a separate study characterizing chemical properties of the ash samples used here, Santín *et al*. (2015) have pointed to the increasing contribution of charred top soil to the ash layer with increasing fire severity as the most feasible explanation for the positive relationship observed here between ash loads and fire severity. This hypothesis agrees with the positive relationship between mean soil charring depth and fire severity observed for two small wildfires in the greater Sydney area (Chafer, 2008).

Previous studies have examined the spatial distribution of wildfire-derived ash (Smith and Hudak 2005; Goforth *et al*. 2005; Kokaly *et al*. 2007), but this study is, to the authors' knowledge, the first that quantifies the total amount of ash produced over the entire area burnt by a wildfire. Once the quantity and spatial distribution of ash is known, it is then possible to incorporate the data into risk analysis models, potentially incorporating terrain and rainfall factors to determine which drainage lines may become conduits for suspended material in the event of a heavy post-wildfire rainfall event. More generally, ash-impacts on soil properties, water contamination and risk could also be addressed (Smith *et al.* 2011; Bodí *et al.* 2014)**.**

The methodology proposed here has proven to be useful in the present case study; however, more research is required to validate the outcomes reported. Published spectral reflectance curves from both Landsat and hyperspectral platforms and laboratory results indicate that wildfire ash from different forested environments around the world have similar reflectance

properties (Landmann 2003; Lewis *et al.* 2006; Kokaly *et al*. 2007; Smith *et al*. 2010; Lewis *et al*. 2011; Brook *et al.* 2015), which suggests that this method should be applicable elsewhere. Important requirements are (i) access to the burnt area for sampling soon after fire, given that ash can soon be redistributed after wildfire (Bodí *et al*. 2014) and (ii) availability of suitable cloud-free and smoke-free satellite imagery acquired pre-fire and close to the time of field sampling. Once robust relationships between fuel, fire parameters and ash loads as measured in the field have been established for a given region, satellite image analysis could be used as a stand-alone tool

Conclusions

This manuscript has shown that by using spectral signatures in the near- and short-wave infrared bands derived from satellite imagery, the spatial distribution and estimated load of ash (t ha^{-1}) can be successfully modelled within a GIS framework. The 'Normalised Wildfire Ash Index' (NWAI) introduced here (as a modification of the NDII), had a significant field-based empirical and spatially modelled correlation with post-wildfire ash loads across a range of fire severities (R^2=0.98). It was found that the highest ash loads were found in areas impacted by the highest wildfire severities as determined using the standard dNBR. This novel approach has yet to be tested for other wildfires and in other environments; however, its underlying principles should be widely applicable. The ability to estimate the loads and spatial distribution of ash present after wildfire is not only of direct relevance to water supply catchment managers in terms of understanding potential risk to water quality, as is the case for the study area examined here. The approach developed here could also be the first critical step in enabling ash load to be introduced as a new parameter into post-fire risk models and assessments.

Acknowledgements

This work has been supported by the WaterNSW (formerly Sydney Catchment Authority), The Leverhulme Trust (Grant Nr. RPG-2014-95) and Swansea University (SU). This paper reflects the authors' views and not necessarily those of the WNSW or SU. We thank three anonymous referees for suggestions that improved this manuscript.

275

276 **References**

277 Balfour VN, Doerr SH, Robichaud PR (2014) The temporal evolution of wildfire ash and
278 implications for post-fire hillslope hydrology. *International Journal of Wildland Fire*
279 **23**, 733-745.

280 Bodí M B, Mataix-Solera J, Doerr SH, Cerdà A (2011). The wettability of ash from burned
281 vegetation and its relationship to Mediterranean plant species type, burn severity and
282 total organic carbon content. *Geoderma* **160**, 599–607.

283 Bodí MB, Martin DA, Balfour VN, Santín C, Doerr SH, Pereira P, Mataix-Solera J, Cerdà, A.
284 (2014). Wildland fire ash: production, composition and eco-hydro-geomorphic
285 effects. *Earth-Science Reviews* **130**, 103-127.

286 Brook A, Hamzi S, Wittenberg L (2015) Wildfire ash: chemical composition, ash-soil
287 interaction and environmental impacts. *Geophysical Research Abstracts* **17**
288 **EGU2015-734**

289 Chafer CJ (2008) A comparison of fire severity measures: An Australian example and
290 implications for predicting major areas of soil erosion. *Catena* **74**, 235-245.

291 Chafer CJ, Noonan M, Macnaught E (2004) The post-fire measurement of fire severity and
292 intensity in the Christmas 2001 Sydney wildfires. *International Journal of Wildland*
293 *Fire* **13**, 227–240.

294 Datt B (1999) Remote sensing of water content in Eucalyptus leaves. *Australian Journal*
295 *Botany* **47**, 909-923.

296 Doerr SH, Shakesby RA, Blake WH, Humphreys GS, Chafer CJ, Wallbrink PJ, (2006)
297 Effects of differing wildfire severity on soil wettability in Australian eucalypt
298 catchments. *Journal of Hydrology* **319**, 295-311.

299 Earth explorer. http://earthexplorer.usgs.gov (accessed on 02/02/2015).

300 FAO (2014) World Reference Base for Soil Resources 2014. *World Soil Resources Report*
301 *106.* Food and Agriculture Organization of the United Nations. Rome.

Goforth BR, Graham RC, Hubbert KR, Zanner CW, Minnich RA (2005) Spatial distribution and properties of ash and thermally altered soils after high severity forest fire, southern California. *International Journal of Wildland Fire* **14**, 343-354.

Hardisky MA, Klemas V, Smart RM (1983) The influence of soil salinity, growth form and leaf moisture on the spectral reflectance of *Spartina alierniflora* canopies. *Photogrammetric Engineering & Remote Sensing* **49**, 77-83.

Hexagon (2015) Erdas Imagine 2014. Hexagon Geospatial Co. Hintsville, Alabama, USA

Hudak AT, Ottmar RD, Vihnanek RE, Brewer NW, Smith AMS, Morgan P (2013) The relationship of post-fire white ash cover to surface fuel consumption. *International Journal of Wildland Fire* **22**, 780–785.

Keith DA (2006) Ocean Shores to Desert Dunes: the native vegetation of New South Wales and the ACT. Department of Environment and Conservation (NSW), Sydney, Australia.

Key CH (2006). Ecological and sampling constraints on defining landscape fire severity. *Fire Ecology* **2**, 34-59.

Kokaly RF, Rockwell BW, Haire SL, King TVV (2007) Characterizing of post-fire surface cover, soils and burn severity at the Cerro Grande Fire, New Mexico, using hyperspectral and multispectral remote sensing. *Remote Sensing of Environment* **106**, 305-325.

Landmann T (2003) Characterizing sub-pixel Landsat ETM+ fire severity on experimental fires in the Kruger National Park, South Africa. *South African Journal of Science* **99**, 357-360.

Lewis SA, Hudak AT, Ottmar RD, Robichaud PR, Lentile LB Hood SM, Cronan JB, Morgan P (2011) Using hyperspectral imagery to estimate forest floor consumption from wildfire in boreal forests of Alaska, USA. *International Journal of Wildland Fire* **20**, 255-271.

Lewis SA, Lentile LB, Hudak AT, Robichaud PR, Morgan P, Bobbitt MJ (2007) Mapping ground cover using hyperspectral remote sensing after the 2003 Simi and Old wildfires in southern California *Fire Ecology* **3**, 109-128.

Lugassi R, Ben-Dor E, Eshel G (2009) Heat-induced soil mineralogical changes, as monitored by reflectance spectral information. *Proceedings 6th EARSeL Imaging Spectroscopy SIG Workshop*, Tel Aviv, Israel.

Malvar MC, Prats SA, Nunes JP, Keizer JJ (2011) Post-fire overland flow generation and inter-rill erosion under simulated rainfall in two eucalypt stands in north-central Portugal. *Environmental Research* **111,** 222–236.

Moody JA, Shakesby RA, Robichaud PR, Cannon SH, Martin DA (2013) Current research issues related to post-wildfire runoff and erosion processes. *Earth-Science Review,* **122**, 10–37.

Murphy J (2014) Hall Road Fire. *Bush Fire Bulletin* **20,** 27-29

NASA (2010) The Landsat Continuity Mission http://landsat.gsfc.nasa.gov/pdf_archive/20101119_LDCMbrochure.pdf (accessed on 02 December 2013)

Pereira P, Úbeda X, Martin DA, Mataix-Solera J, Cerdà A, Burguet M (2014). Wildfire effects on extractable elements in ash from a *Pinus pinaster* forest in Portugal. *Hydrological Processes* **28**, 3681–3690.

Santín C, Doerr SH, Shakesby RA, Bryant R, Sheridan GJ, Lane PNJ, Smith HG, Bell TL (2012) Carbon forms and sequestration potential within ash deposits from forest fires: new insights from the 2009 'Black Saturday' fires, Australia. *European Journal of Forest Research* **131**, 1245-1253.

Santín C, Doerr SH, Otero XL, Chafer CJ (2015) Quantity, composition and water contamination potential of ash produced under different wildfire severities. *Environmental Research* **142**, 297-308.

Shakesby RA, Doerr SH (2006) Wildfire as a hydrological and geomorphological agent. *Earth-Science Review* **74,** 269-307.

360 Shakesby RA, Wallbrink PJ, Doerr SH, English PM, Chafer C, Humphreys GS, Blake WH,
361 Tomkins KM (2007) Distinctiveness of wildfire effects on soil erosion in south-east
362 Australian eucalypt forests assessed in a global context. *Forest Ecology and*
363 *Management* **238**, 347-364.

364 Smith AMS, Hudak AT (2005) Estimating combustion of large downed woody debris from
365 residual white ash. *International Journal of Wildland Fire* **14**, 245-248.

366 Smith AMS, Eitel JUH, Hudak AT (2010) Spectral analysis of charcoal on soils: implications
367 for wildfire severity mapping methods. *International Journal of Wildland Fire* **19**,
368 976-983.

369 Smith HG, Sheridan GJ, Lane PNJ, Nyman P, Haydon S (2011) Wildfire effects on water
370 quality in forest catchments: a review with implications for water supply. *Journal of*
371 *Hydrology* **396**, 170-192.

372 USGS (2015) Using the USGS Landsat 8 Product.
373 http://landsat.usgs.gov/Landsat8_Using_Product.php (accessed on 02 February 2014)

374 Vincentie H (2012) Ash unraveled: a descriptive study about physical, chemical and spectral
375 characteristics of ash and soil in a Mediterranean forest after a large wildfire at Mount
376 Carmel, Israel. MSc Thesis, Wageningen University, Netherlands

377 Wang L, Hunt, ER, Qu JJ, Hao, X, Daughtry, CST. (2013) Remote sensing of fuel moisture
378 content from ratios of narrow-band vegetation water and dry-matter indices. *Remote*
379 *Sening of Environment* **129**, 103-110.

380 Yilmaz MT, Hunt ERJr, Jackson TJ (2008) Remote sensing of vegetation water content from
381 equivalent water thickness using satellite imagery. *Remote Sensing of Environment*
382 **112**, 2514-2522.

383

384

Preprint of accepted manuscript: Chafer, C., Santin, C. & Doerr, S.H. (2016) Modelling and quantifying the spatial distribution of post-wildfire ash loads. *International Journal of Wildland Fire* 25, 249-255. (*doi:10.1071/WF15074*).

Figures

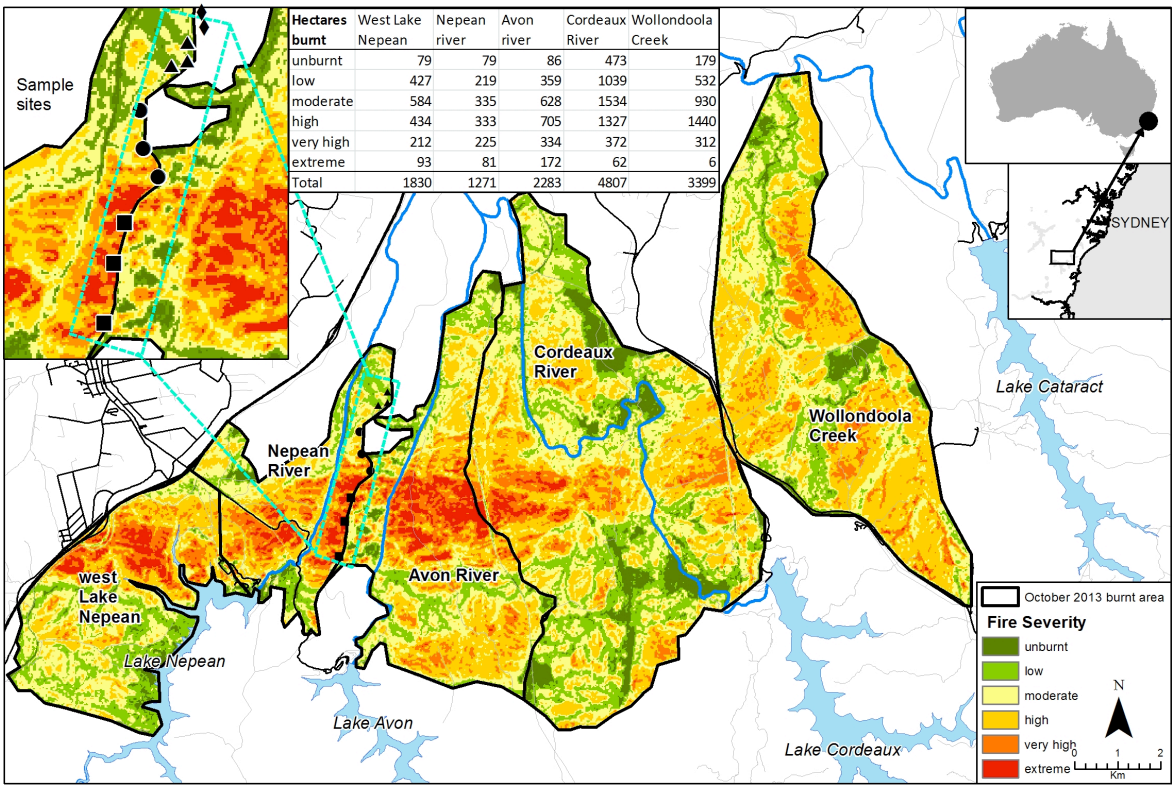

Figure 1. Study area, fire severity classes, location of sampling sites and total area burnt for each severity class in the five subcatchments affected by the Hall Road wildfire (October 2013, ~100km SW of Sydney, Australia: Lat -34.31, Long 150.68 degrees). Sampling sites are shown in the upper left (triangles ▲: extreme severity sites; squares ■: high severity sites; circles ●: low severity sites; diamonds ♦: unburnt site). The table shows the burnt area (ha) for each severity class within each of the five subcatchments.

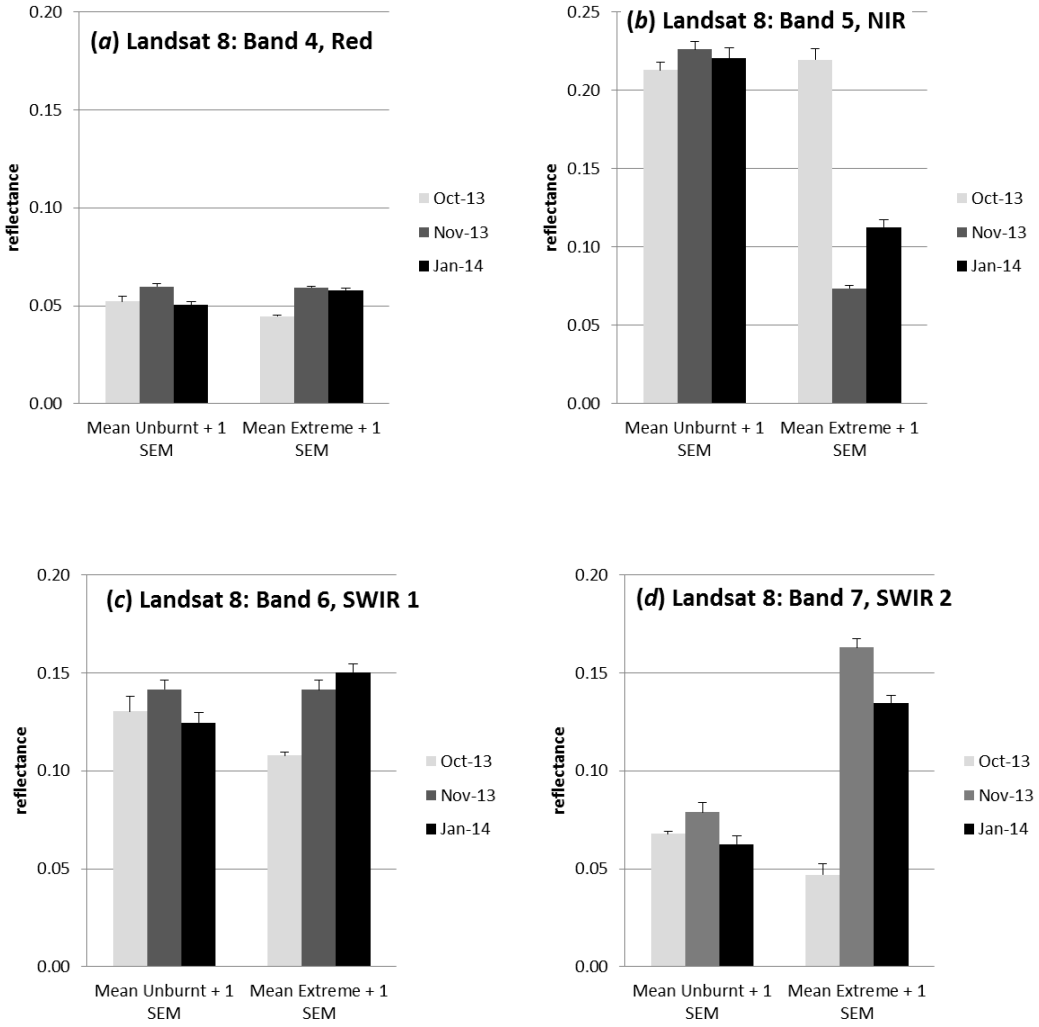

Figure 2. Spectral differences (reflectance +1 standard error of the mean - SEM) from the sample sites for unburnt and extreme severity data only. Data is for four spectral bands (*a*) Red, (b) NIR, (c) SWIR-1 and (*d*) SWIR-2 respectively from the Landsat 8 satellite images covering the 0.63-2.30 micron range for three images covering the study area before (October 2013) and after the Hall Road wildfire (November 2013 and January 2014). Thus, for the NDWI used herein, NIR and SWIR-1 are used.

Preprint of accepted manuscript: Chafer, C., Santin, C. & Doerr, S.H. (2016) Modelling and quantifying the spatial distribution of post-wildfire ash loads. *International Journal of Wildland Fire* 25, 249-255. (*doi:10.1071/WF15074*).

406

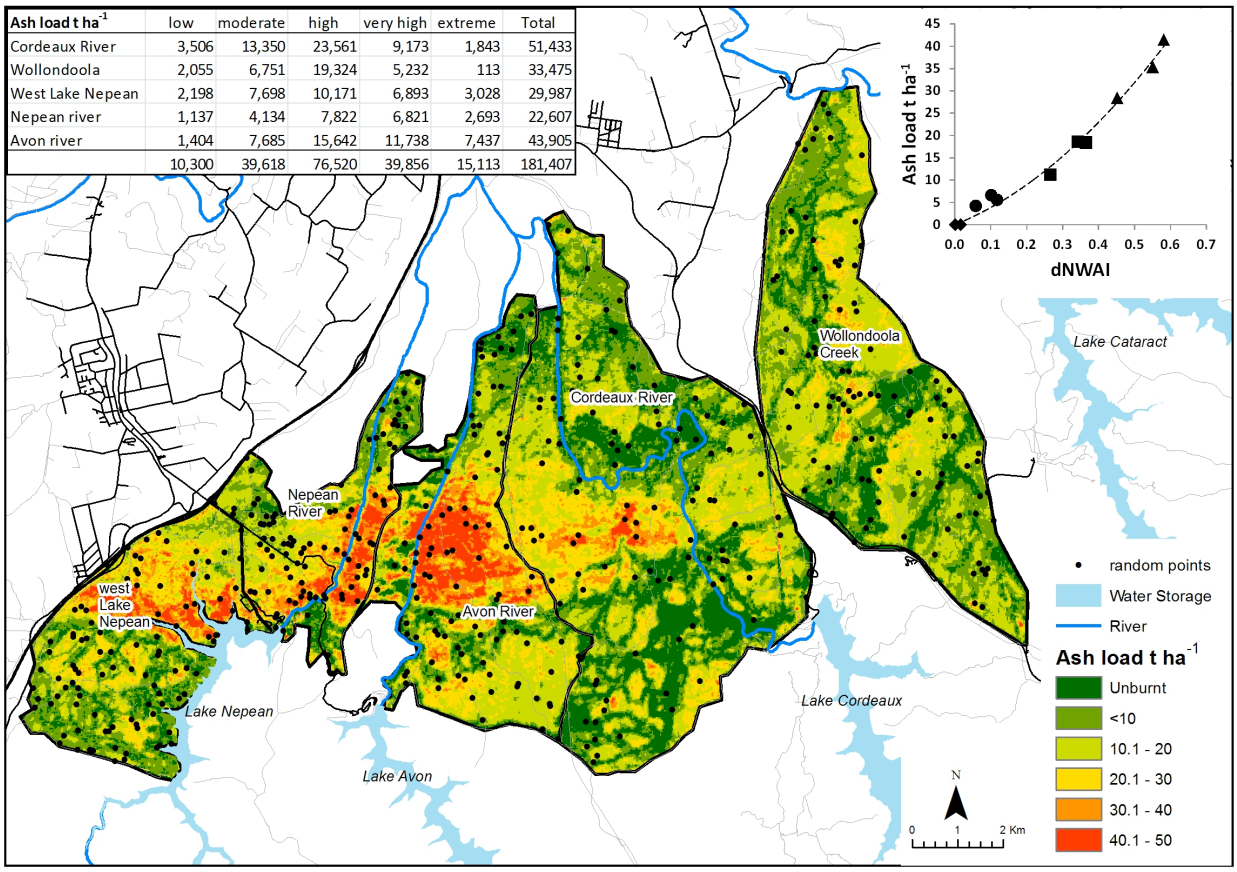

407

408 Figure 3. Spatial distribution of 500 random points and estimated post-wildfire ash loads in
409 tons ha^{-1} for each fire severity class in the five drainage units for the Hall Road wildfire
410 (October 2013, ~100 km SW of Sydney, Australia). Top right: the relationship between the
411 field-measured ash load (tons ha^{-1}) and dNWAI from the nine sampling sites and two unburnt
412 control sites(triangles ▲: extreme severity sites; squares ■: high severity sites; circles ●: low
413 severity sites; diamonds ♦: unburnt sites), ($y=62.9x^2 + 32.3x$, $R^2=0.98$, n=30 per sample site).
414 The table shows the estimated ash load (t ha^{-1}) within each fire severity class within the five
415 subcatchments of the area burnt.
416